PERGAMON

Brief communication

On gas–liquid two-phase flow regimes in microchannels

M.K. Akbar, D.A. Plummer, S.M. Ghiaasiaan [*]

G.W. Woodruff School of Mechanical Engineering, Georgia Institute of Technology, Atlanta, GA 30332-0405, USA

1. Introduction

Gas–liquid two-phase flow patterns in small channels have been investigated rather extensively in the past (Suo and Griffith, 1964; Barnea et al., 1983; Damianides and Westwater, 1988; Barajas and Panton, 1993; Fukano and Kariyasaki, 1993; Mishima et al., 1995, 1996 and Triplett et al., 1999; Coleman and Garimella, 1999; Yang and Shieh, 2001; Zhao and Bi, 2001). In microchannels with near-circular cross-sections, when the hydraulic diameter is smaller than some threshold (approximately $D_H \leqslant 1$ mm with air and water like fluids, with D_H representing the hydraulic diameter) the buoyancy effect is suppressed by surface tension. With the exception of stratified flow, which does not occur due to suppression of buoyancy, however, other major flow patterns that are common in large channels occur in microchannels as well, although certain flow pattern details may be different from those in larger channels (Suo and Griffith, 1964; Damianides and Westwater, 1988; Triplett et al., 1999; Coleman and Garimella, 1999; Yang and Shieh, 2001; Zhao and Bi, 2001). The widely used two-phase flow regime maps and semi-analytical regime transition models, furthermore, overall appear to do rather poorly when compared with microchannel data (Triplett et al., 1999; Ghiaasiaan and Abdel-Khalik, 2001).

There is an important resemblance between two-phase flow in microchannels and in common large channels at microgravity. In both system types the surface tension, inertia, and the viscosity are important, while buoyancy is suppressed. Consequently, two-phase flow regime maps that have previously been developed for microgravity, or at least their underlying methodology, can be useful for microchannels.

The objectives of this study were to: (a) compare and assess the available experimental data that deal with two-phase flow regimes in microchannels; (b) examine the feasibility of a simple Weber number-based two-phase flow regime map following the methodology previously applied by Zhao and Rezkallah (1993) and Rezkallah (1996) to microgravity; and (c) identify areas where further experiments are needed.

[*] Corresponding author. Tel.: +1-404-894-3746; fax: +1-404-894-8496.
E-mail address: seyed.ghiaasiaan@me.gatech.edu (S.M. Ghiaasiaan).

2. Two-phase flow in microchannels and in microgravity

For adiabatic, steady-state, and developed gas–liquid two-phase flow in a smooth pipe, assuming immiscible and incompressible phases, the important variables are ρ_L, ρ_G, μ_L, μ_G, σ, D, g, θ, ϕ, U_{LS}, and U_{GS}, where subscripts L and G represent liquid and gas, respectively, ρ is density, μ is viscosity, σ represents the surface tension, D is the channel diameter, θ is the channel angle of inclination with respect to gravity force, ϕ is the contact angle, g is the gravitational acceleration, and U_{LS} and U_{GS} are the liquid and gas superficial velocities, respectively. Since there are three relevant fundamental dimensions (time, length and mass), eight independent dimensionless parameters can be defined. The independent dimensionless parameters can be chosen as: $\Delta\rho/\rho_L$ (where $\Delta\rho = \rho_L - \rho_G$), θ, ϕ, and

$$Eo = \frac{\Delta\rho g D_H^2}{\sigma} \tag{1}$$

$$We_{LS} = \frac{U_{LS}^2 D_H \rho_L}{\sigma} \tag{2}$$

$$We_{GS} = \frac{U_{GS}^2 D_H \rho_G}{\sigma} \tag{3}$$

$$Re_{LS} = U_{LS} D_H / \nu_L \tag{4}$$

$$Re_{GS} = U_{GS} D_H / \nu_G \tag{5}$$

where ν is the kinematic viscosity, and Eo, We, and Re stand for Eötvös, Weber and Reynolds numbers, respectively. Other relevant and widely used dimensionless parameters include the Bond number, $Bo = D_H/\sqrt{\sigma/(g\Delta\rho)}$; Capillary number, $Ca = \mu_L U_{LS}/\sigma$; phase Froude numbers, $Fr_{GS} = U_{GS}^2/(gD_H)$ and $Fr_{LS} = U_{LS}^2/(gD_H)$; Ohnesorge number $\Gamma = \mu_L/(\sigma D_H \rho_L)^{\frac{1}{2}}$; and Suratman number $Su = \sigma \rho_L D_H/\mu_L^2$. These can all be derived by manipulating and/or combining the aforementioned dimensionless parameters.

In a class of microchannels of interest to a wide range of applications, $Eo < 1$; at least one of the Weber numbers is of the order of 1–10^2; and $Re_{LS} \geqslant 1$; whereby the surface tension dominates buoyancy while inertia is important. Similar conditions, however, apply to the two-phase flow in microgravity as well, indicating that important similarities between two-phase flow processes in the two system categories should be expected.

Zhao and Rezkallah (1993), Rezkallah (1996), and more recently Lowe and Rezkallah (1999) developed two-phase flow transition models for microgravity channel flows based on phasic Weber numbers. Based on the argument that inertia and surface tension are the dominant forces in microgravity two-phase flow, Zhao and Rezkallah used the phasic Weber numbers $We_L = U_L^2 D\rho_L/\sigma$ and $We_G = U_G^2 D\rho_G/\sigma$ (where U_L and U_G are phase velocities) as the most appropriate dimensionless parameters for the correlation of the flow regime transitions. Furthermore, they argued that the entire flow regime map can be divided into three zones: the surface tension dominated zone, including bubbly and slug regimes, where surface tension effect predominates inertia; the inertia-dominated zone, including annular flow regime, where inertia is significantly larger than the surface tension force; and the transition zone, where inertial and surface tension forces are comparable. In view of the difficulty associated with the calculation of phase velocities,

however, they cast their regime transition models using We_{LS} and We_{GS}. Zhao and Rezkallah (1993) suggested $We_{GS} \approx 1$ as the upper bound for surface tension-dominated zone, and $We_{GS} \approx 20$ as the lower bound for the inertia-dominated zone. Revisions were subsequently made by Rezkallah (1996) and Lowe and Rezkallah (1999), whereby the $We_{GS} = \text{const}$ transition lines were replaced with transition lines approximately following $We_{GS} \propto We_{LS}^{0.25}$.

In microchannels operating within the aforementioned parameter range of interest, similar to the microgravity case, surface tension and inertial forces are likely to determine, or at least play significant roles with respect to the flow regimes and their transitions. The role of viscosity is likely to be more important in microchannels, however. Nevertheless, some useful similarities between the flow regime transitions in microchannels and channels operating under microgravity conditions should be expected.

3. Experimental data

Table 1 is a summary of the available relevant experimental investigations utilized in this study. In some of these investigations two or more channel diameters were used. However, only experimental data representing near-circular channels for which $D_H \lesssim 1.5$ mm are shown. In such channels, with air/water-like fluids, flow regimes are insensitive to the channel orientation when $D_H \lesssim 1.0$ mm. This is in approximate agreement with the following criterion proposed by Suo and Griffith (1964) for negligible buoyancy effect: $Bo^{1/2} \lesssim 0.3$, or equivalently, $D_H \lesssim 0.3\lambda$ where $\lambda = \sqrt{\sigma/(g\Delta\rho)}$ represents the Laplace length scale. Significantly larger channels, as well as narrow rectangular or annular flow passages, lack the afore-mentioned distinct microchannel characteristics and will not be considered. Some experimental data dealing with air–water and steam–water flow in much smaller round channels ($D = 10$–100 μm) have been performed by Serizawa and Feng (2001). These data show complicated flow patterns some of which are different than those common in channels in the 1-mm range. The major regimes included bubbly, slug (dominated by large gas plugs), liquid ring (a regime characterized by a contiguous gas core with a periodic structure that includes thick, ring-like, annular liquid films), liquid lump (a regime dominated by discrete liquid lumps), and liquid droplet flow (similar to the aforementioned froth flow regime). Other, more complicated flow regimes have also been observed by Serizawa et al. These data will not be addressed, since they evidently deal with a channel size range outside the range of interest here. Some important attributes of the experiments listed in Table 1 of particular interest here are briefly mentioned.

The data of Triplett et al. (1999) were obtained with air and water at near-atmospheric pressure and room temperature, in circular channels with 1.1 and 1.45 mm inner diameter test sections, and in microchannels with semi-triangular (equivalent triangular with one corner smoothed) cross-sections with 1.09 and 1.49 mm hydraulic diameters. Flow patterns and flow pattern maps were overall similar for the two channel cross-section geometries. Barajas and Panton (1993) were concerned with the effect of surface wettability on flow regimes in microchannels, and used air and water at room conditions, in microchannels made of different materials such that contact angles in the 34–106° range were obtained. Overall, the flow regime transition lines were relatively insensitive to the contact angle when the contact angle was in the $\theta \leqslant 74°$. With $\theta = 106°$, however, the regime transition lines were significantly displaced. Furthermore, wavy and annular flow patterns

Table 1
Summary of experimental data used in the present study

Source	Test section characteristics	Fluids	Pressure and temperature	Gas superficial velocity (m/s)	Liquid superficial velocity (m/s)	Observed flow patterns
Damianides and Westwater (1988)	1.0 mm I. D. Horizontal glass tube	Air–Water	Atmospheric pressure and 20 °C	0.715–55.3	0.0095–1.53	Dispersed-bubbly, Bubbly, Plug, Slug, Pseudo-slug, Dispersed-droplet, and Annular
Barajas and Panton (1993)	1.6 mm I. D. 34° Inclined horizontal	Air–Water	Room conditions (Atmospheric pressure and 25 °C)	0.1–100.0	0.003–2.0	Bubbly, Dispersed, Plug, Slug, Annular, Wavy; and Rivulet for partially non-wetting conditions
Mishima et al. (1995)	1.05 mm I. D. Vertical round tube	Air–Water	Room conditions	1.0–80.0	0.5–20.0	Slug and Annular
Coleman and Garimella (1999)	1.3 mm I. D. Horizontal round tube	Air–Water	Room conditions	1.0–100	0.1–10.0	Bubbly, Plug, Slug, Wavy-annular, Annular, and Dispersed
Triplett et al. (1999)	1.1 mm I. D. Horizontal round tube; Semi-triangular channel with $D_H = 1.1$ and 1.49 mm	Air–Water	Room conditions	0.04–100.0	0.04–8.0	Bubbly, Slug, Churn, Slug-annular, and Annular
Yang and Shieh (2001)	1.0 mm I. D. Horizontal round tube	Air–Water	Room conditions	0.21–75.0	0.014–1.34	Bubbly, Plug, Slug, Slug-annular, Annular, and Dispersed
Zhao and Bi (2001)	0.866 and 1.443 mm D_h Equilateral triangular vertical channel	Air–Water	Room conditions	0.1–100.0	0.1–10.0	Bubbly, Slug, Churn, Annular; and Capillary-bubbly in the smaller channel

were partly replaced with rivulets in tests with large contact angles. Their data representing $\theta = 34°$ (which were similar to their data with $\theta = 74°$) are used here.

Zhao and Bi (2001) used equilateral triangular-cross section channels with $D_H = 0.87$, 1.44 and 2.89 mm, and observed the occurrence of all major flow regimes. Their smallest test section supported, however, a novel capillary-bubbly flow pattern at very low liquid superficial velocities, characterized by a single train of ellipsoidal bubble. Mishima et al. (1995) used vertical test sections with $D_H = 1.05$–4.08 mm. With their smallest channel, they only identified slug and annular flow patterns, however.

4. Flow regime maps

In accordance with the above discussion, we divide the entire flow regime map into four regions.

(a) The surface tension-dominated region, including bubbly, plug, and slug (where a flow pattern dominated by large and elongated bubbles is meant).
(b) Inertia-dominated zone 1, including annular and wavy-annular regimes.
(c) Inertia-dominated zone 2, including the dispersed flow regimes.
(d) Transition zone.

As mentioned earlier, microgravity two-phase flow patterns have been divided into three groups: surface tension dominated; inertia dominated; and transition. Careful review of the microchannel data, however, indicates that the above-mentioned four flow regime zones can be easily defined.

Comparison among the microchannel two-phase flow regime data is complicated and due to the inconsistent terminology used by various authors for some flow patterns (Triplett et al., 1999; Ghiaasiaan and Abdel-Khalik, 2001). Thus, in the above division of flow patterns distinction is made between slug flow regime, when it is defined as the pattern dominated by elongated, large bubbles (e.g. in Damianides and Westwater, 1988); and the flow pattern that represents transition from plug to annular flow, and is characterized by large waves superimposed on an otherwise separated phases that intermittently block the channel (e.g., Yang and Shieh, 2001). Also, the flow pattern referred to as churn flow by Triplett et al. (1999) in fact included two different regimes according to most of the other investigators: churn flow characterized by unstable and aerated long bubbles similar to the pseudo-slug regime as defined by Suo and Griffith (1964) and frothy-slug defined by Zhao and Rezkallah (1993); and churn flow characterized by churning waves and froth. The latter flow pattern, furthermore, appears to have been identified as dispersed flow by some of the other investigators (Damianides and Westwater, 1988; Barajas and Panton, 1993; Coleman and Garimella, 1999; Yang and Shieh, 2001). In view of the apparent inconsistency regarding the latter flow pattern, it will be addressed as froth flow in the forthcoming discussions. In the figures, however, ''(dispersed)'' will be included in reference to this flow regime.

Zhao and Bi (2001) identified a churn flow pattern based on pressure fluctuation characteristics which occupied a transition zone between slug and annular flow patterns. Comparison with the experimental data of Damianides and Westwater (1988), Triplett et al. (1999), and others,

however, shows that Zhao and Bi's churn flow may be the same as the slug-annular regime of the latter investigators, and the wavy-annular regime of others.

Figs. 1 and 2 display the transition lines representing the boundaries among the aforementioned flow regime zones, in U_{LS} vs. U_{GS}, and We_{LS} vs. We_{GS} coordinates, respectively. Only the data that represent near-circular microchannels with $D_H \leqslant 1$ mm are depicted, and other data sets will be discussed shortly. With the exception of the data of Mishima et al. (1995) and Zhao and Bi (2001), all other data in the figures are in overall agreement. Mishima et al. (1995) only distinguished slug and annular regimes in tests with their smallest channel, apparently disregarding the flow patterns that represent transition between slug and annular flow regimes. The churn–slug transition line of Triplett et al. (1999) also is not shown since, as explained earlier, the churn flow region of Triplett et al. in fact included the dispersed flow and the flow pattern characterized by aerated long bubbles. The latter flow pattern is included in the transition zone here, however. The discrepancy among the data with respect to regime transition lines are at least partly a result of the uncertainty in visually distinguishing subtle regime variations, which is particularly difficult at low liquid flow rates. The data of Zhao and Bi (2001) will be discussed shortly. The overall good agreement among the displayed data with respect to the aforementioned major flow patterns supports the feasibility of an empirical flow regime map. Figs. 1 and 2 show that flow regime transition lines can be easily defined using either coordinate system. Weber number coordinates, which are dimensionless and utilize the potential similarity with microgravity, may be more appropriate. It should, however, be emphasized that the transition zone in the flow regime maps covers a number of complex and subtle flow patterns, including the aerated-slug and pseudo-slug flows, and
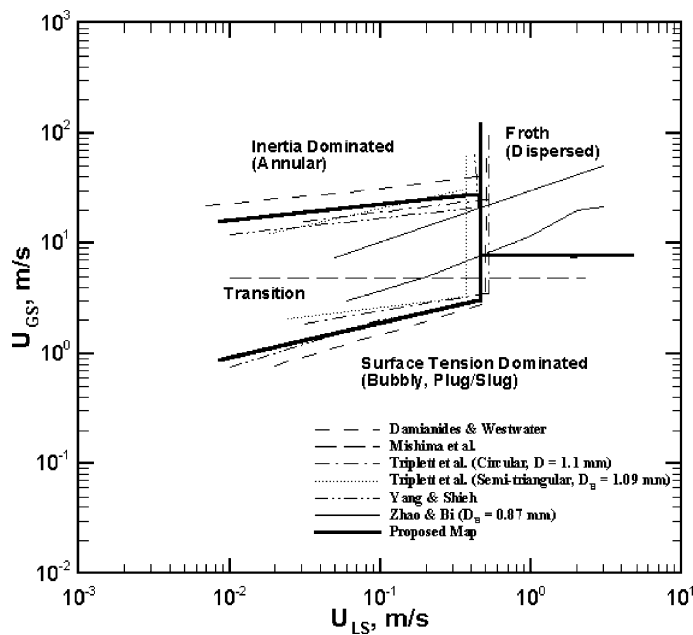
Fig. 1. Flow regime transition lines for circular and near-circular channels with $D_H \leqslant 1$ mm, using superficial velocities as coordinates.
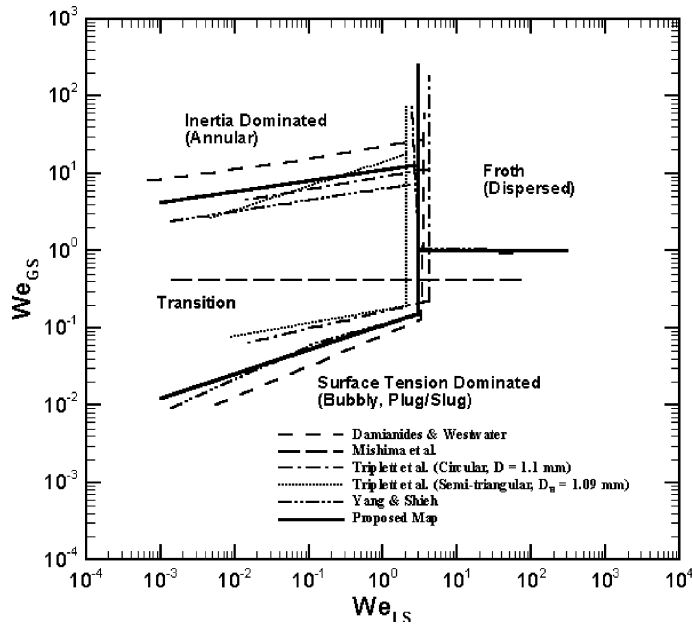
Fig. 2. Flow regime transition lines for circular and near-circular channels with $D_H \leqslant 1$ mm, using Weber numbers as coordinates.

possibly others. Detailed characterization of these flow regimes and their transitions is difficult due to the scarcity of data.

The regime transition lines fitted to all relevant data for air–water flow in circular and near-circular microchannels with $D_H \lesssim 1.0$ mm, and recommended for regime transition predictions, are also depicted in Fig. 2, and can be represented by the following expressions:

- Surface tension dominated zone:
    - For $We_{LS} \leqslant 3.0$:

$$We_{GS} \leqslant 0.11 We_{LS}^{0.315} \tag{6}$$

    - For $We_{LS} > 3$:

$$We_{GS} \leqslant 1.0 \tag{7}$$

- Annular flow zone (inertia dominated zone 1):

$$We_{GS} \geqslant 11.0 We_{LS}^{0.14} \tag{8a}$$

$$We_{LS} \leqslant 3.0 \tag{8b}$$

- Dispersed flow zone (inertia dominated zone 2):

$$We_{LS} > 3.0 \tag{9a}$$

$$We_{GS} > 1.0 \tag{9b}$$

Two major influences with the aforementioned microgravity two-phase flow regime maps can be emphasized. First, the slopes of the regime transition lines between the surface tension-dominated and inertia-dominated zones and the transition zone are different from the approximate $We_{LS} \propto We_{GS}^{0.25}$ relation that applies to microgravity (Lowe and Rezkallah, 1999). More importantly, a frothy flow region can be easily defined and its borders correlated here. It represents conditions when the liquid and gas inertias are comparable, and may be attributable to the relative importance of liquid viscous effects in microchannels.

5. Effects of channel hydraulic diameter, geometry, and orientation

All the displayed data in Fig. 1, as noted earlier, represent air–water flow in circular and near-circular (triangular with one corner smoothed) channels with $D_H \leqslant 1$ mm. Therefore, the flow regime model proposed in the previous section should be applied to other geometric and flow conditions with caution. To better illustrate the potential weaknesses of the proposed method, the effects of channel size and cross-section geometry are now discussed. It is emphasized, however, that the range of interest is limited to $D_H \lesssim \lambda/2$.

The flow regime transition lines of Triplett et al. (1999) for their semi-triangular channel with $D_H = 1.49$ mm, Barajas and Panton (1993), and Coleman and Garimella (1999) for their test sections with $D_H = 1.3$ mm, are shown in Figs. 3 and 4, and are compared with the average transition lines obtained with smaller test sections. Flow regimes are depicted in We_{LS} vs. We_{GS} conditions only, for brevity. The trends to be discussed are similar when U_{LS} and U_{GS} coordinates are used, however. Also depicted in the figures are the relevant regime transition lines of Zhao and Bi (2001) representing their data with $D_H = 1.44$ mm. Fig. 4 indicates that the mean regime transition line representing the transition zone–surface tension dominated zone regime change (Eq. (6)) is in good overall agreement with the data. Only fair agreement can also be noted with respect to the transition zone–annular zone boundary (Eq. (8)), however. The available data disagree with respect to the boundaries of the dispersed flow regime zone, furthermore, and no clear and consistent trend can be deduced from the data. Complications associated with the exact definition of this flow regime may cause the apparent disagreement. More experiments are evidently needed before the effect of channel size can be ascertained, and incorporated in the regime transition expressions if needed.

The effect of channel cross-section geometry can also be assessed by comparison among the data of Zhao and Bi (2001), Triplett et al. (for their semi-triangular channels), and the remainder of the data. The transition lines of Zhao and Bi (2001) for their smaller test section deviates from the remainder of the date in Fig. 2, and suggests that the flow patterns in a triangular test section with sharp corners may in fact be different than the flow patterns in a circular channel with a diameter equal to its hydraulic diameter.

Most of the experimental studies dealing with two-phase flow in near-circular microchannels have used horizontal test sections, and insensitivity of flow regimes and their transition boundaries to channel orientation has been expected (Ghiaasiaan and Abdel-Khalik, 2001). The data of
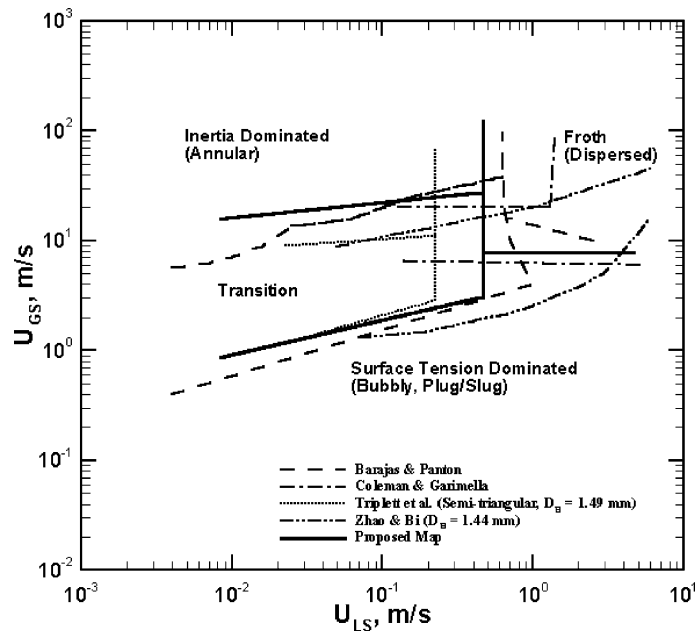
Fig. 3. Flow regime transition lines for circular and near-circular channels with $D_H > 1$ mm, using superficial velocities as coordinates.
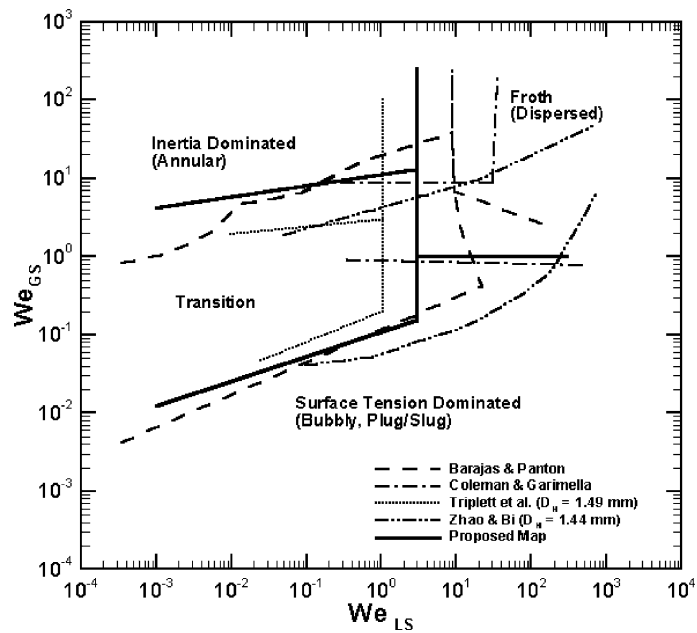
Fig. 4. Flow regime transition lines for circular and near-circular channels with $D_H > 1$ mm, using Weber numbers as coordinates.

Zhao and Bi (2001), however, appear to indicate the absence of froth (dispersed) flow in their vertically orientated test section, in disagreement with virtually all other data.

6. Summary and concluding remarks

1. For $D_H \leqslant 1$ mm channel size range, the available data for near-circular microchannels and air–water like fluid pairs, are in reasonable agreement. For these conditions, a simple Weber number-based flow regime map that divides the entire map into four zones (surface tension-dominated, annular, froth, and transition) could be devised.
2. For $D_H > 1$ mm, the aforementioned flow regime map is in fair agreement with available data, with the exception of the boundaries of the froth (dispersed) flow regime zone.
3. The limited available data indicate that triangular channels with sharp corners may support somewhat different regimes and transition boundaries than near-circular channels.
4. Systematic experiments addressing the effects of channel cross-section size and geometric configuration are needed.
5. Virtually all available data represent air/water and air/water-like fluid pairs at room conditions. The potential effects of fluid properties are thus unknown, and systematic experimental studies using other fluids are needed.

References

Barajas, A.M., Panton, R.L., 1993. The effect of contact angle on two-phase flow in capillary tubes. Int. J. Multiphase Flow 19, 337–346.

Barnea, D., Luninski, Y., Taitel, Y., 1983. Flow in small diameter pipes. Can J. Chem. Engng. 61, 617–620.

Coleman, J.W., Garimella, S., 1999. Characteristics of two-phase patterns in small diameter round and rectangular tubes. Int. J. Heat Mass Transfer 42, 2869–2881.

Damianides, C.A., Westwater, J.W., 1988. Two-phase flow patterns in a compact heat exchanger and in small tubes. In: Proc. Second UK National Conf. On Heat Transfer, Glasgow, 14–16 September. Mechanical Engineering Publications, London, pp. 1257–1268.

Fukano, T., Kariyasaki, A., 1993. Characteristics of gas–liquid two-phase flow in a capillary. Nucl. Eng. Design 141, 59–68.

Ghiaasiaan, S.M., Abdel-Khalik, S.I., 2001. Two-phase flow in microchannels. Adv. Heat Transfer 34, 145–254.

Lowe, D.C., Rezkallah, K.S., 1999. Flow regime identification in microgravity two-phase flow using void fraction signals. Int. J. Multiphase Flow 25, 433–457.

Mishima, K, Hibiki, T., Nishihara, H., 1995. Some characteristics of air–water two-phase flow in small diameter tubes. Proc 2nd Int. Conf. Multiphase Flow, Vol. 4, April 3–7, 1995, Tokyo, Japan, pp. 39– 46.

Mishima, K., Hibiki, T., 1996. Some characteristics of air–water two-phase flow in small diameter vertical tubes. Int. J. Multiphase Flow 22, 703–712.

Rezkallah, K.S., 1996. Weber number based flow-pattern maps for liquid–gas flows at microgravity. Int. J. Multiphase Flow 22, 1265–1270.

Serizawa, A., Feng, Z.P., 2001. Two-phase flow in microchannels. Proc. 4th International Conf. Multiphase Flow, May 27–June 1, 2001, New Orleans, LA, USA.

Suo, M., Griffith, P., 1964. Two-phase flow in capillary tubes. J. Basic Eng. 86, 576–582.

Triplett, K.A., Ghiaasiaan, S.M., Adbel-Khalik, S.I., Sadowski, D.L., 1999. Gas–liquid two-phase flow in microchannels. Part I: Two-phase flow patterns. Int. J. Multiphase Flow 25, 377–394.

Yang, C.Y., Shieh, C.C., 2001. Flow pattern of air–water and two-phase R-134a in small circular tubes. Int. J. Multiphase Flow 27, 1163–1177.

Zhao, L., Rezkallah, K.S., 1993. Gas–liquid flow patterns at microgravity conditions. Int. J. Multiphase Flow 19, 751–763.

Zhao, T.S., Bi, Q.C., 2001. Co-current air–water two-phase flow patterns in vertical triangular microchannels. Int. J. Multiphase Flow 27, 765–782.